



Influence of the Experimental Setup on the Damping Properties of SLM Lattice Structures

F. Scalzo¹  · G. Totis² · M. Sortino²

Received: 5 May 2022 / Accepted: 22 August 2022
© The Author(s) 2022

Abstract

Background Metal lattice structures obtained through Selective Laser Melting may increase the strength-to-weight ratio of advanced 3D printed parts, as well as their damping properties. Recent experimental results showed that AISi10Mg and AISI 316L lattices are characterized by higher Rayleigh damping coefficients with respect to the fully dense material. However, some unclear or contradictory results were found, depending on the experimental setup adopted for modal analysis.

Objective In this work the influence of the experimental setup when performing modal analysis on different SLM AISI 316L lattice structures was deeply investigated. The study provides a critical comparison of various experimental modal analysis approaches, allowing to evaluate the influence of external damping sources and material internal damping phenomena.

Methods The dynamic behaviour of SLM AISI 316L specimens incorporating lattice structures was estimated by means of pulse testing and sinusoidal excitation through an electromagnetic shaker. The validity of the viscous damping model was assessed by means of sinusoidal excitation with different levels of vibration velocity. Moreover, the influence of experimental setup on modal analysis results was critically evaluated, by considering different actuators, contact and non-contact sensors and boundary/clamping conditions.

Results The classical viscous damping model describes with good approximation the damping properties of SLM lattice structures. When exciting single specimens in free-free conditions, those embedding lattice structure and unmelted metal powder filler were characterized by superior internal damping properties with respect to the specimens incorporating the lattice structure without any filler, which was however more effective than the full density equivalent material. Most of the other experimental setups introduced additional external damping sources, that could alter this important outcome.

Conclusions SLM lattice structures embedded into 3D printed components provide superior damping properties against mechanical and acoustic vibrations and the metal powder filler does significantly enhance such damping capacity. A correct estimation of material internal damping was achieved by applying non-contact sensors and free-free boundary conditions, whereas other experimental setups were partly inadequate.

Keywords Lattice structure · Selective laser melting · Vibrations · Modal analysis · Damping

Introduction

Modern additive manufacturing (AM) allows to overcome many of the typical disadvantages of traditional subtractive techniques. 3D solid parts are produced by means of layer-by-layer material addition, allowing to obtain lightweight components with good mechanical performances, complex geometries, faster engineering and production times and easy production delocalization. Cutting-edge industry such as aerospace, automotive, defence, medical, and energy already take advantage of the benefits of AM for high performance applications [1].

✉ F. Scalzo
federico.scalzo@dia.units.it

G. Totis
giovanni.totis@uniud.it

M. Sortino
marco.sortino@uniud.it

¹ Department of Engineering and Architecture, University of Trieste, Via Alfonso Valerio 6, Trieste 34127, Italy

² Polytechnic Department of Engineering and Architecture, University of Udine, Via delle Scienze 206, Udine 33100, Italy

By exploiting the superior design freedom of AM, it is possible to enhance the performances of 3D printed parts with respect to similar components obtained by subtractive technologies. Several strategies can be applied for this purpose. For instance, topology optimization methods were applied in [2, 3], giving rise to complex designs resembling biological structures.

Another strategy involves the use of three-dimensional porous structures formed by the ordered repetition of unit cells with a given geometry, called lattice structures [4]. By adequately selecting the topology and the geometrical characteristics of the unit cell, it is possible to improve its mechanical, thermal and vibro-acoustic performances. Hence, these structures have been successfully applied to obtain materials with variable local mechanical properties [5–7], high strength lightweight components [8, 9], improved impact absorption capacity [10, 11], enhanced heat exchange capabilities [12, 13], increased damping against mechanical vibrations and improved vibro-acoustic isolation [14–16].

Contrary to the chaotic cellular structures of metallic foams, 3D printed lattices are optimized engineered materials that are fabricated with good accuracy and repeatability [17]. Among AM techniques, Selective Laser Melting (SLM) can be successfully applied to achieve superior thermo-mechanical performances. It is a Powder Bed Fusion (PBF) AM technique that allows manufacturing of 3D metallic parts starting from gas-atomized powders, spread layer-upon-layer, selectively scanned and melted by a laser energy source. Lattice structures with good mechanical properties and geometric accuracy can be produced by SLM. On the contrary, other AM techniques such as Direct Metal Deposition (DMD) are not suitable for this application [18].

The vast majority of studies investigating lattice structures focus on mechanical properties assessment by means of tensile/compressive [19, 20], impact [21, 22] or fatigue testing [23]. Moreover, microstructural characterization by means of Scanning Electron Microscopy (SEM) and Micro Computed Tomography (μ CT) is quite common [24–26].

Conversely, the dynamic behaviour of lattice structures has not been extensively studied yet. Andresen et al. [27] applied an evolutionary strategic optimization to maximize the first eigenfrequency of SLM AlSi10Mg lattices, helping to prevent resonance phenomena. Rosa et al. [28] demonstrated that SLM BCC lattices made of AISI 316L have better damping performances with respect to equivalent bulk reference specimens. The authors suggested that this behaviour could be due to the superimposition of amplitude independent and amplitude dependent internal friction phenomena. Moreover, presence of cracks and surface defects could give an additional contribution to the overall damping capacity of the structure as suggested also by Haghshenas and Khonsari [29].

Sortino et al. [30] performed an experimental modal analysis (EMA) on SLM AlSi10Mg lattices. Specimens made of unit cells with FBCCZ topology and different cell and strut size were investigated by means of pulse testing, thus proving their better damping properties with respect to the reference material. The same authors did considerably extend this investigation to AISI 316L SLM lattice structures in [31], by also producing and testing specimens having different sizes. As a result of this research, a scale-independent Rayleigh model describing the observed viscous damping properties for each lattice type was successfully validated.

These results inspired an innovative method for passive vibrations suppression in milling of thin-walled parts [32]. In that work, three similar blade-like fixtures were 3D printed by means of SLM and then compared in terms of their dynamic behaviour: a full density blade, a blade embedding a given lattice structure and a third configuration having the same lattice structure filled with unmelted metal powder. The latter was found to be the most effective against mechanical vibrations, both during modal analysis and cutting tests. No significant differences were found between the first and second configuration, contrary to the expectations derived from [32]. A possible explanation of this behaviour will be provided in this work.

Recently, Hong et al. [33] demonstrated that SLM AlSi10Mg lattice structures filled with tin-bismuth alloy can be engineered in order to maximise their damping properties, thus generating a complete bandgap in the low-frequency range that can be useful for several advanced applications. Sun et al. [16] developed a new strategy to prepare an aluminium matrix composite (AMC) with enhanced damping properties. The AMC was an AlSi10Mg-NiTi lattice structure interpenetrating phase composite (IPC) produced exploiting additive manufacturing (AM) and vacuum infiltration process. The IPC's damping capacity and compressive strength were almost double compared with those of AlSi10Mg reference material. The damping capacity improvement was mainly due to the interface damping phenomena with the combined effects of grain boundary damping and stacking faults. Li et al. [34] proposed a strategy to achieve broadband low-frequency vibration attenuation in 3D printed composite meta-lattice sandwich structures. Broadband low-frequency vibration bandgaps were conceived exploiting the characteristics of locally resonant metamaterials and lightweight lattice sandwich structures. Two kinds of meta-lattice sandwich panels were 3D printed and the vibration suppression performance and bandgap generation mechanisms were investigated. The coupling between the designed secondary structures and host panels allowed to achieve enhanced vibration suppression properties. Liu et al. [35] investigated the compressive behaviour and vibration-damping properties of 3D printed Ti6Al4V porous structures. Transition between elasto-brittle and

elasto-plastic behaviour was observed by increasing the cell size. Moreover, the compressive performances were closely related to the porous structure relative density. The energy absorption capability increased linearly with as-manufactured density. The energy absorption efficiency was influenced by both the cell geometry and the cell size. The cellular structure with larger cell size had better damping properties compared to the smaller sized one. Wang et al. [36] studied the effects of ageing and thermal cycling on the microstructure and vibration damping of a porous CuAlMn shape memory alloy. Ageing temperature influenced both material's microstructure and internal friction peak. Moreover, thermal cycling affected the porous structure's damping behaviour. Damping performance gradually increased at ambient temperature, starting to decrease again when more than twenty thermal cycles were exceeded.

Estimation of the vibration damping properties of mechanical structures is not an easy task. In addition to the internal material damping, many other external dissipative phenomena and error sources are present, which may considerably affect the estimated global damping, as it was pointed out in [37].

Specifically:

- joint damping due to energy dissipation at mechanical interfaces between the examined specimen and external environment;
- air or fluid-structure viscous interaction;
- energy dissipation through contact sensors;
- special uncontrolled environmental conditions;
- improper measurement, inadequate excitation configuration and excessive noise.

Since the observed damping is the sum of all these effects acting at the same time, it is very difficult to accurately quantify the material internal damping.

The aim of this work is to provide a more accurate and reliable estimate of material internal damping for a given lattice type with and without metal powder filler in comparison to a full density equivalent material. Moreover, the influence of the experimental configurations on the obtained results will be investigated. In detail, the damping properties of SLM manufactured lattice structures made of AISI 316L austenitic stainless steel were investigated here, in order to achieve the following objectives:

1. an accurate characterization of the material internal damping corresponding to different SLM lattice types and macroscopic specimens' geometries, by minimizing the influence of external dissipative phenomena;
2. an experimental proof of the adequacy of the viscous damping hypothesis;

3. an experimental evidence that only when specimens are suspended in free-free conditions the internal damping can be correctly identified, whereas the other experimental configurations and boundary conditions are responsible for undesired disturbances that may alter the final results of the modal analysis.

The paper is structured as follows. In the next section the different experimental configurations, boundary conditions and tested specimens will be presented. Then, the experimental data will be analysed and the main results will be discussed. Eventually, conclusions will be drawn in the final section.

Specimen Design and Production

According to the results of the previous experimental campaigns [31, 32], SLM lattice structures can be very effective for mechanical energy dissipation, especially when unmelted powder filler is retained within the lattice porosities. However, this behaviour was not confirmed by all the experimental data, likely because of the influence of some external additional dissipative phenomena.

Here some beam-like and blade-like specimens were further investigated under different boundary conditions and by using several experimental setups with the aim of better evidencing the internal damping from all the other dissipative mechanisms. By so doing, the superior damping properties of SLM lattice structures should clearly emerge.

Specimens Geometry

Beam-like and blade-like specimens' geometries were conceived in order to facilitate the dynamic behaviour assessment of different kinds of lattice structures metamaterials, ensuring that the lattice contribution to the overall specimen mechanic behaviour was significant. Furthermore, these geometries are very similar to a wide variety of mechanical components that can benefit from the use of high performance metamaterials, allowing the study of their static and dynamic mechanical performance. The beam-like shaped specimens are representative of structural elements and members of mechanical systems, robotic mechanisms and tools, while the blade-like shaped ones are representative of slender structures such as turbine blades, parts for aerospace applications and thin mechanical components in general. The beam-like and blade-like geometries were designed by means of SolidWorks Simulation and ANSYS Mechanical APDL FEA [31, 32] in order to satisfy different objectives and constraints:

- specimens should be designed to achieve a reference global static stiffness;
- the dominant resonances should be located at low-medium frequencies;
- it should be possible to clamp the specimens in different configurations, preventing lattice damage and allowing external excitation;
- specimens should comply with SLM manufacturing constraints (e.g. build volume, minimum feature size, overhangs, support removal).

The final specimens' geometry complies with each constraint and allows the analysis both in cantilever and free-free configurations. A comparison between different experimental setups and constraint conditions was therefore possible, allowing to evaluate the effect of lattice global geometry and clamping conditions on specimen's dynamics.

Beam-like specimens had a square cross section of 21x21 mm and an axial length of 130 mm. Each specimen was composed by three sections: a full density lower base, a central section embedding a given lattice structure and a full density upper base. A lattice made of FBCCZ topology cubic unit cells with 2 mm cell size and 0.4 mm strut diameter was chosen due to its promising damping behaviour combined with adequate manufacturability [31]. Three different kinds of metamaterials were evaluated:

- open lattice structure mentioned above (L);
- the same lattice structure closed by an external thin shell trapping unmelted metal powder (P);
- full density section providing the same bending static compliance, for comparison (R).

The blade-like specimens had a lower base designed for mechanical clamping on machine tool table, a central section embedding the same lattice structure of the beam-like specimens (with and without metal powder) and an upper base where a sacrificial sample could be clamped. All the geometrical details of the blade-like specimens can be found in [32]. In the current case, the upper base was used for the application of the external force. Modal parameters of both

bending and torsional modes were evaluated here under different configurations, in order to shed light on the partly unexpected behaviour observed in previous work.

The specimens' geometrical characteristics and section views are shown in Table 1.

Specimens SLM 3D Printing

SLM manufacturing of the specimens required STL 3D model preparation, positioning, support design and slicing that were fulfilled with Materialise Magics software. The SLM 3D printing process was carried out with a Concept Laser M2 Cusing, selecting Argon to inertize the working chamber. AISI 316L metal powder with the following particle size distribution (PSD) was used: $d_{10} = 19.8 \mu\text{m}$, $d_{50} = 29.9 \mu\text{m}$, $d_{90} = 45.1 \mu\text{m}$. The powder chemical composition was 17.7% Cr, 12.9% Ni, 2.39% Mo, 1.31% Mn, 0.66% Si, 0.016% C and balance Fe.

The main process parameters were set as follows: laser power 180 W, scan speed 600 mm/s, spot diameter 120 μm and layer thickness 25 μm .

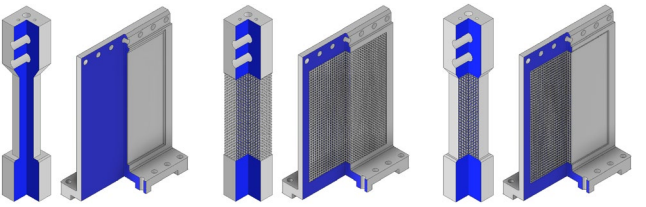
Specimens were heat treated by maintaining them at 550 °C for six hours, and then by gradually cooling them in air at room temperature. This treatment is a standard procedure for partially relieving the thermal stresses and thus reducing thermal distortion of 3D printed parts.

The specimens were further machined by using a CNC milling machine at the surfaces that were clamped in the cantilever configurations, in order to improve the contact conditions at the mechanical interfaces/fixtures and to reduce any undesired slippage or friction. The final post-processed specimens are shown in Fig. 1.

It is worth recalling that the considered lattice geometry was affected by non-negligible geometrical errors, as pointed out by the instrumental optical inspection reported in [31, 32]. Inclined strut diameters were larger than the nominal value due to SLM process related conditions such as the staircase effect, poor heat conduction near overhanging surfaces and unwanted adhesion of partially melted powders. Nevertheless, these systematic geometrical errors are not

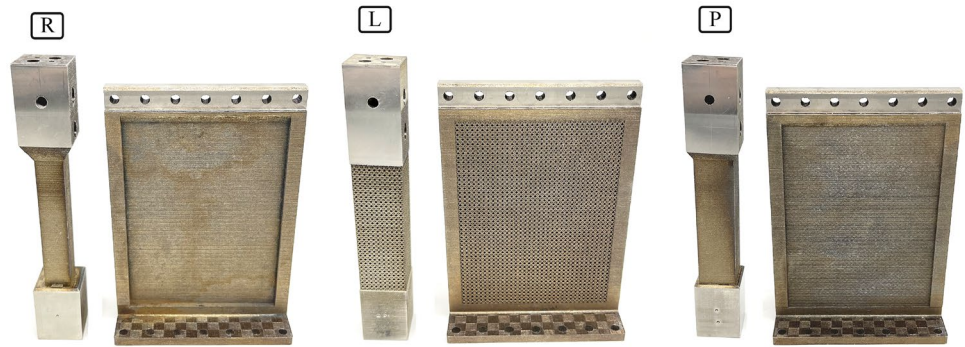
Table 1 Specimens under investigation

Properties	Reference (R)	Lattice(L)	Lattice with raw pow. (P)
Unit cell topology	Full cross section	FBCCZ	FBCCZ
Unit cell size [mm]	-	2	2
Strut diameter [mm]	-	0.4	0.4



Specimens' geometry

Fig. 1 Specimens after stress relieving heat treatment and milled contact surfaces



important in this work, also thanks to the good geometrical repeatability among similar specimens.

Experimental Setups and Testing Conditions

The specimens were tested with different experimental setups, that are illustrated in the following paragraphs. For each constraint configuration, the excitation point was chosen on the basis of the indications provided by the finite element analysis, in order to favour the excitation of the dominant mode. From a mechanical point of view, the dominant mode is particularly interesting as it contributes significantly to the vibration of the structure. Lattice structure deformation is mostly due to the dominant mode of vibration. The peculiar geometric and mechanical characteristics of the beam-like and blade-like specimens made it possible to capture the low-medium frequency dynamic behaviour of lattice meta-materials, under both bending and torsional loading conditions. Moreover, each specimen was analysed under different testing conditions allowing for a thorough evaluation of the influence of the experimental setup on the lattices’ damping properties.

Impulsive Excitation in Cantilever Configuration

Beam-like specimens were clamped in cantilever configuration on a vice (Gerardi 640 Type 2), that was further fixed on the rotary table of a Haas VF2-TR CNC milling machine, as done in [31].

An impact hammer Dytran 5800B4 was used to provide the external impulsive force F_{inp} , while the vibration U was measured by a non-contact eddy current probe Micro Espi-son ES1, as illustrated in Fig. 2. Signals were acquired with a National Instrument NI9215 module with a sampling rate equal to 50 kHz and elaborated within MathWorks MATLAB environment.

The same experiment was repeated for the blade-like specimens analysed in [32]. The pulse test (PT) was repeated 12 times for each specimen. Transients’ length was selected

in order to assure a good signal to noise ratio. A low-pass filter at 10 kHz was applied before sampling.

Afterwards, the final dynamic compliance and coherence function were estimated through cross-spectrum and auto-spectrum relations.

Parametric dynamic models composed of single or multiple harmonic oscillators were finally estimated by means of the Impulse Dynamic Subspace (IDS) method [38], thus allowing the identification of natural frequencies and damping ratios of the dominant vibration modes.

Harmonic Excitation by Using an Electromagnetic Shaker

An asymmetric single beam cantilever configuration could not be excited by using an electromagnetic shaker. A symmetric configuration was needed for this purpose. This was

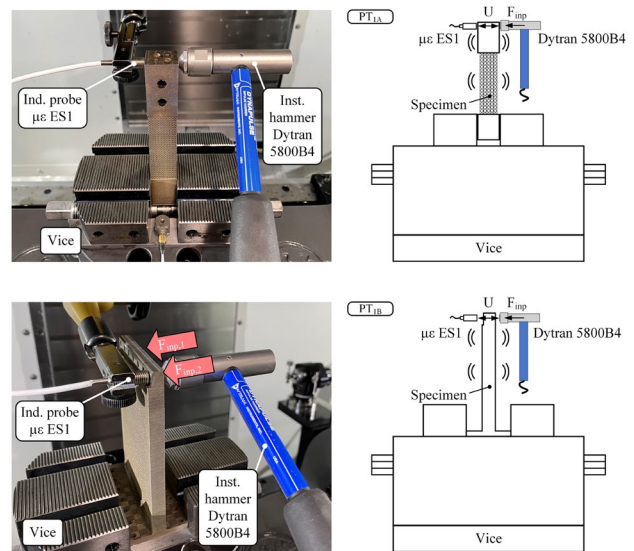


Fig. 2 Experimental setup for modal analysis of beam-like specimens in cantilever conditions at a vice (PT_{1A} , top). Experimental setup for modal analysis of blade-like specimens in similar conditions (PT_{1B} , bottom)

possible by considering a double beam configuration comprising two aligned specimens clamped together at their adjacent extremities. The first natural vibration of such double beam configuration was approximately the same of the single cantilever beam [39]. Hence, this configuration was well suited for comparison with the single cantilever specimens.

In detail, two replicates of each specimen were clamped by means of a special fixture. Preliminary tests showed that the clamping force greatly influenced the damping losses. Thus, the clamping device screws were tightened up to 9 Nm with a torque wrench.

The central clamping device of the double beam configuration was further screwed to a Bruel & Kjaer 4809 electrodynamic shaker.

Two Kistler 8704B accelerometers (sensitivity 100 mV/g) were attached to the beam free tips to monitor their vibrations. A Kistler 8763B accelerometer (sensitivity 50 mV/g) was screwed on the clamping device in order to monitor its vibration.

A frequency sweep/chirp excitation was applied by the shaker by varying the main frequency in the surroundings of the first resonance peak and by also controlling - at any frequency - the amplitude of the relative vibration velocity between the free tips and the central node of the system. Figure 3 shows the S_1 setup and a schematic view highlighting sensors' positioning.

The sinusoidal chirp was generated by a National Instruments NI9263 module, that was amplified by a Bruel & Kjaer 2718 power amplifier and eventually fed to the electrodynamic shaker. Specimens dynamic compliance was calculated as the ratio of the tip-base relative displacement and the inertial force applied on tip due to the resulting tip acceleration, i.e.

$$W(j\omega) = \frac{U_1(j\omega) - U_2(j\omega)}{F_{1,in}(j\omega)} = \frac{\frac{A_1(j\omega)}{(j\omega)^2} - \frac{A_2(j\omega)}{(j\omega)^2}}{-m_1 A_2(j\omega)} \quad (1)$$

where $U_1(j\omega)$ and $U_2(j\omega)$ are the tip and centre displacements, while $F_{(1,in)}(j\omega)$ is the inertial force due to the modal mass m_1 vibration. Displacements were calculated by integrating the

Table 2 Vibration velocity DoE factors and levels

Factor	Levels	Values
Specimen type	3	Full density cross section (R), Lattice (L), lattice with powder (P)
Vibration velocity [m/s]	2	0.004, 0.008
Replicates (by disassembling and re-assembling the specimens)	4	-
Experimental setup	2	Accelerometers, accel. & las. disp. sensor

accelerometers' signals in the frequency domain as done in the right hand side of equation (1), where $A_1(j\omega)$ and $A_2(j\omega)$ are the tip and centre accelerations, respectively.

The natural frequency and the damping ratio of the dominant mode were estimated by fitting the observed resonance peak with a single mass-spring-damper model by means of least-squares estimation in the frequency domain.

Two different levels of vibration velocity were tested to evaluate its influence on the damping ratio. Table 2 summarizes the adopted Design of Experiments (DoE).

Measurements were replicated four times, by mounting and dismounting the specimens from the clamping device and by controlling the clamping force through the torque wrench. The accelerometers calibration coefficients were slightly corrected to respect the rigid body motion hypothesis at low frequencies.

Afterwards, a non-contact Micro-Epsilon LD 1605-2 laser triangulation displacement sensor was used in order to eliminate the undesired energy dissipation caused by accelerometers wires. The S_2 experimental setup is shown in Fig. 4.

As done before, sensors calibration was adjusted through the rigid body motion assumption at low frequency. Four replicates were carried out by mounting and dismounting the specimens and carefully tightening the screws with the torque wrench. Specimens were excited with a sinusoidal chirp, repeating the measurements at 0.004 m/s and 0.008 m/s tip velocities to investigate the effect on damping losses.

Fig. 3 Experimental setup S_1 for harmonic excitation through an electromagnetic shaker and piezoelectric accelerometers for measuring all the inspected nodes

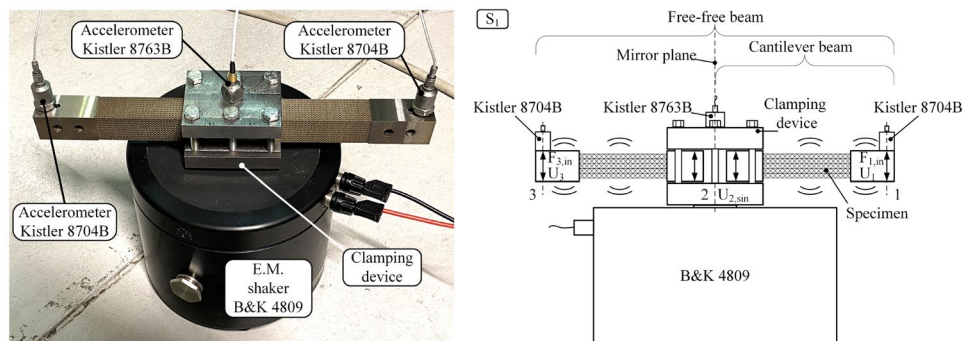
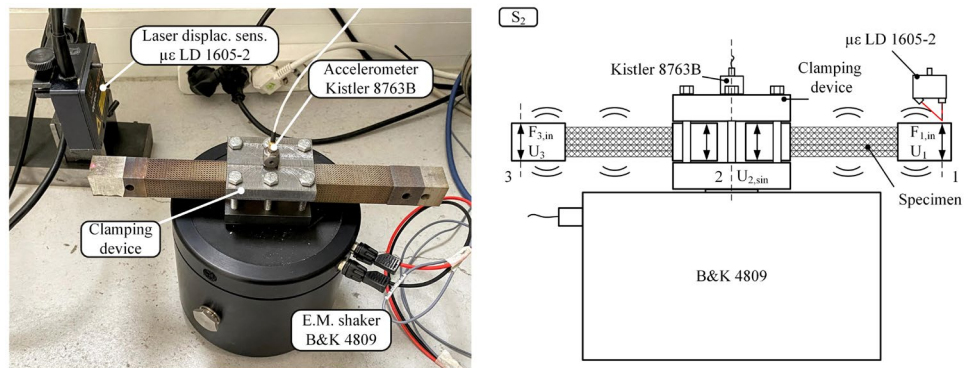


Fig. 4 Experimental setup S_2 for harmonic excitation through an electromagnetic shaker, single central accelerometer and a laser triangulation sensor



Dynamic compliance of each pair of specimens was calculated by using equation (1), where U_1 was already available from the displacement sensor. Again, the dominant natural frequency and the damping ratio were estimated by means of curve fitting as before.

Impulsive Excitation in Free-free Suspended Conditions

To further minimize the influence of the external damping sources, pulse tests were performed in free-free configuration. The beam-like specimens were suspended by using nylon threads positioned at nodes of the dominant mode shape to reduce external damping losses. The impulsive force was applied by the instrumented hammer at the antinode of the dominant vibration mode. The sound pressure field owing to the interaction between the vibrating specimen and air was measured by means of a PCB 377B02 free-field, prepolarized condenser microphone (sensitivity 50 mV/Pa) connected to a PCB 482C15 ICP signal conditioner. The measurements were performed inside an anechoic chamber to minimize the environmental noise.

Experiments were repeated with the double beam symmetrical configuration that was also analysed by the electromagnetic shaker.

Moreover, tests were performed with the blade-like specimens as well, in order to better understand the effects of lattice structure on both bending and torsional vibration modes. Modal parameters were extracted by using the IDS algorithm [38], as done for the pulse tests on the vice in cantilever configuration. PT_{2A} , PT_{2B} and PT_{2C} configurations are shown in Fig. 5.

Results and Discussion

Quite often the effect of external damping sources on damping properties of materials or complex structures is neglected. Therefore, results consistency could be undermined unless the boundary conditions are similar to those of

the experimental campaign. Awareness about the influence of damping losses due to joint energy dissipation, contact making measurement devices and improper fixturing or excitation is important to make the best use of the information obtained from EMA. The dynamic behaviour of the lattice specimens tested in the different experimental conditions and the effect of the external damping sources are reported in the following paragraphs.

Results Obtained from Beam-like Specimens

Firstly, the impact of external damping sources was assessed from the comparison between the results obtained from experimental setups S_1 and S_2 .

Dynamic compliances of the symmetrical beam-like specimens R, L and P clamped on top of the electromagnetic shaker and measured by using accelerometers are illustrated in Fig. 6(a). In this configuration, the resonance frequencies were located in the range 500–600 Hz. The single viscoelastic harmonic oscillator fit well the system response. Under these conditions the resonance peaks associated to the lattice specimens were similar and only slightly lower than the resonance peak corresponding to the full density specimen. No appreciable difference between the damping ratios of lattice and reference specimens was noticeable.

When the accelerometers were replaced by a non-contact triangulation laser probe (Fig. 6(b)), resonance frequencies were all slightly shifted to higher values and all the resonance peaks increased of one order or magnitude. Moreover, the damping ratios were two order of magnitude smaller and it was possible to observe significant differences between the responses of each individual specimen. These variations among apparently similar experimental setups were caused by the relevant load effect introduced by accelerometers' masses and wires. Sensors' choice and positioning could have a very strong impact on the dynamic behaviour of the system under investigation. The damping owing to contact measurement devices is at least two orders of magnitude larger than inherent material damping. Therefore, accelerometers are not recommended for characterizing the

Fig. 5 Vibro-acoustic characterization of specimens suspended in free-free conditions inside an anechoic chamber, by using the instrumented hammer and a free-field microphone. Single beam (PT_{2A} , top), double beam (PT_{2B} , middle) and blade-like (PT_{2C} , bottom) configurations were measured

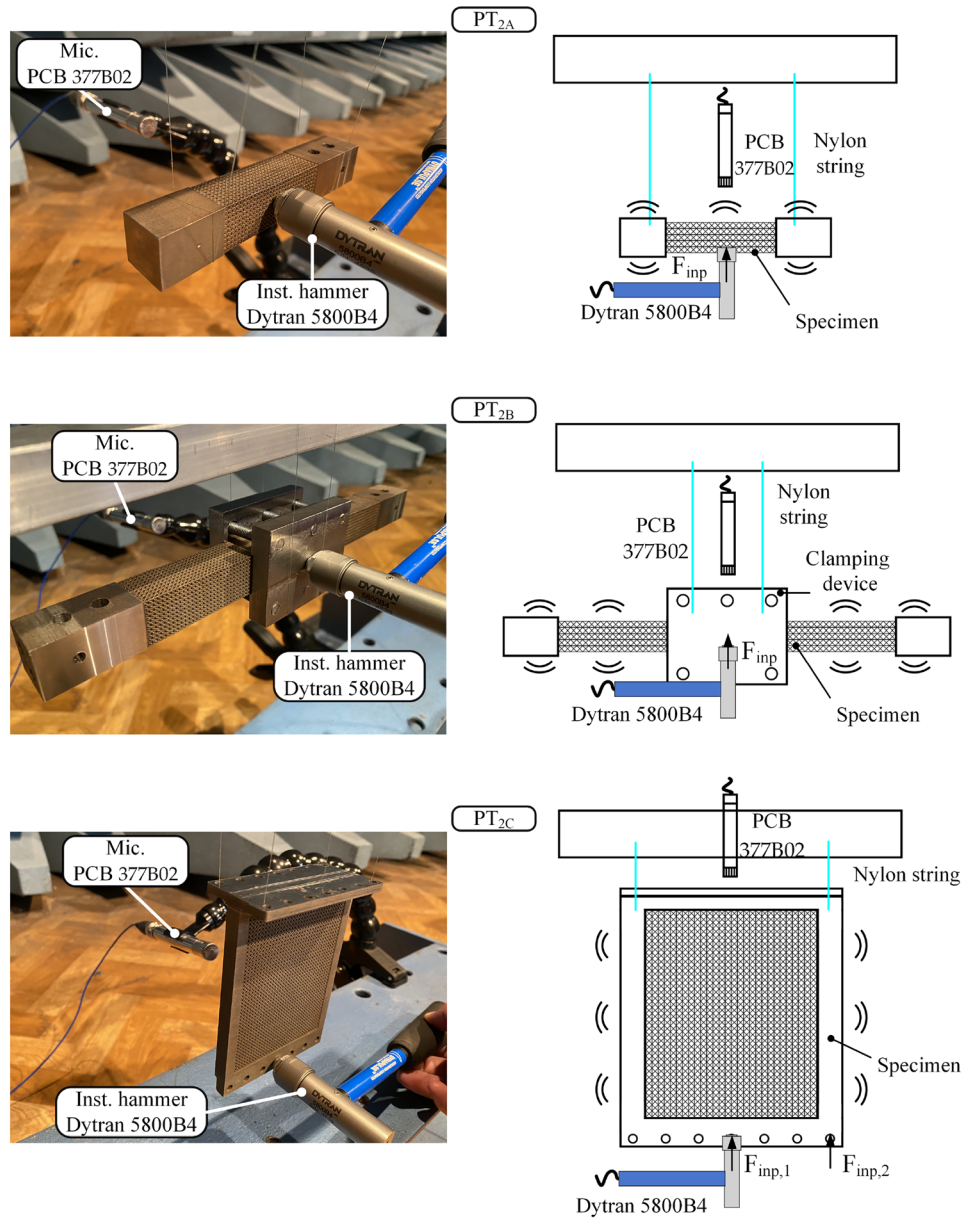
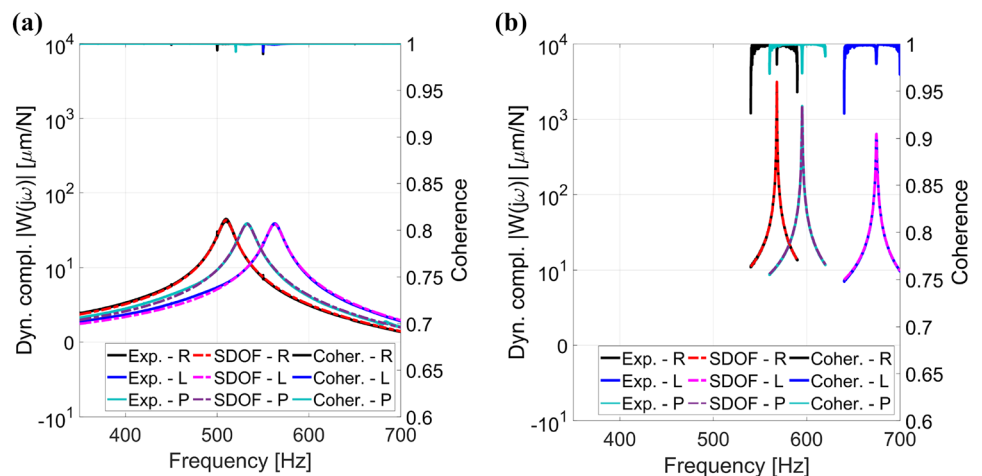


Fig. 6 Reference (R), lattice (L) and lattice + pow. (P) specimens' dynamic compliances obtained with accelerometers (a) or with laser displacement sensor (b)



internal damping of relatively small specimens. This result is in accordance with other authors who performed similar measurements [37, 40]. According to the latter experimental setup, the damping ratio of P is smaller than that of L, contrary to the findings reported in [32], see Fig. 7(b).

When suspending the double symmetric specimen by using wires in the anechoic chamber setup (PT_{2B}), the lattice structure (with and without powder filler) showed superior damping properties with respect to the full density reference specimen.

Nevertheless, there is no significant statistical difference among the lattice types according to the boxplot represented in Fig. 7(c). The equipment used to couple the specimens in the symmetrical configuration caused variable damping losses depending on the contact conditions established during assembly.

When clamping the single specimens in cantilever conditions at the vice (PT_{1A} of Fig. 7(d)), the damping ratios were one order of magnitude higher than those characterizing the double specimens (S_2 and PT_{2B}). The main reason was the larger mechanical energy dissipation at the specimen-vice contact surfaces, where micro sliding, friction and non-linear contact phenomena may occur. These local dissipative sources prevailed on the lattice internal damping under these circumstances. Again, there is no clear statistical difference among the two lattice types in PT_{1A} .

Only when analysing the single specimens suspended in free-free conditions in the anechoic chamber (Fig. 7(a)) the lattice type with powder filler (P) exhibited a significantly superior damping than lattice type without filler (L), which was however superior than the reference full density specimen (R). Under these conditions, the damping ratio of the lattice specimen (L) is five times higher with respect to the reference one (R), while the powder filler gives an additional advantage further tripling the damping ratio with respect to specimen (L).

The influence of the experimental setup on the damping properties of the lattice structures can be further analysed by observing the mean values of damping ratios. As previously mentioned, with free-free boundary conditions (PT_{2A}), the lattice specimens (L and P) have significantly superior damping properties compared to the reference (R). The influence of external damping sources is negligible since no dynamic coupling or dissipative phenomena due to contact surfaces affected the measurement, allowing for a better assessment of the material internal damping. Results obtained with configurations S_2 and PT_{2B} are slightly different with respect to those of PT_{2A} . In both cases the powder filled specimen (P) advantage in terms of damping was hindered. The contact phenomena occurring at the interface between the specimens and the coupling equipment influenced the dynamic behaviour of the structure, making it more difficult to evaluate the inherent material damping contribution. The influence of external damping sources is even more relevant in the case of the PT_{1A} configuration. The dynamic coupling between the specimen and the vice significantly affects the response of the lattice. This is demonstrated by the fact that on average the damping ratio is an order of magnitude larger than that of the other test configurations.

In conclusion the raw metal powder filler undoubtedly enhances the damping capacity of the lattice structure. However, it does also increase the weight to mechanical strength ratio with respect to the plain lattice structure.

This behaviour was definitely proven in free-free conditions, which were the less perturbed by additional dissipative sources.

Different clamping conditions and experimental setups introduced undesired dissipative phenomena that strongly influenced this result.

It is worth noting that the dominant bending mode of the single cantilever beam occurred at about 600 Hz. The

Fig. 7 Beam-like specimens' damping ratio, estimated with different experimental setups

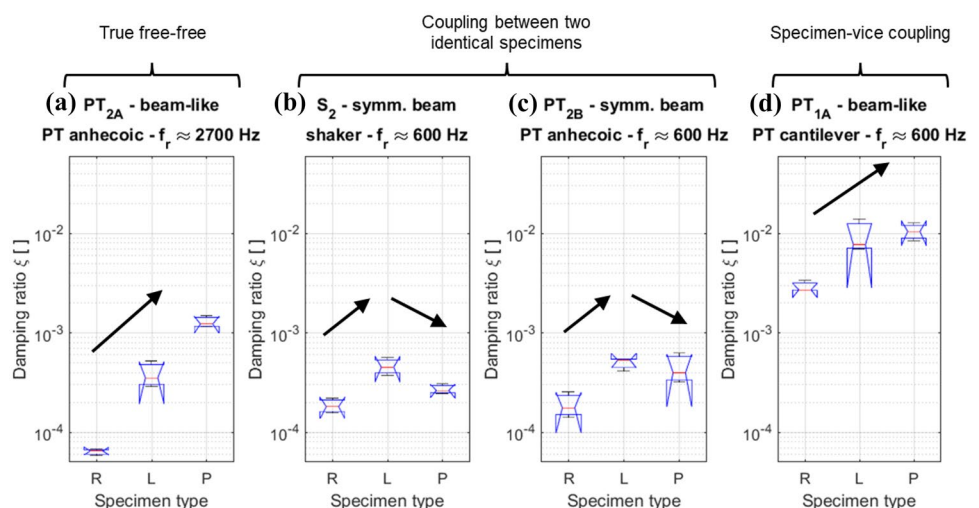


Fig. 8 Dominant mode shape contour plot of S_1 , S_2 , PT_{2B} (a), PT_{1A} (b) and PT_{2A} (c) configurations

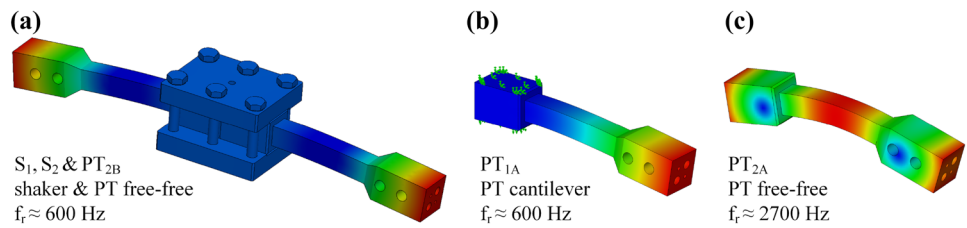


Table 3 Analysis of variance on damping ratio values derived from specimens R, L and P tested in configuration S_2

Factor	Sum Sq.	DoF	Mean Sq.	F	p-value
Specimen type	4.83e-7	2	2.42e-7	74.62	0
Vib. velocity	1.06e-8	1	1.06e-8	3.29	0.0791
Error	1.04e-7	32	3.24e-9		
Total	5.97e-7	35			

same mode was dominant in all the double symmetrical beam configurations. On the other side, the first dominant vibration mode of the single beam suspended in free-free conditions manifested at 2700 Hz. According to FEA simulations (see Fig. 8) all these vibration modes have similar stress-strain fields in the lattice region, thus their damping capacity should be similar unless it is frequency dependent.

To further assess the adequacy of the viscous damping model, a chirp input signal was applied through the shaker by modulating its frequency and amplitude in real time in order to keep a constant (relative) vibration velocity.

According to the analysis of variance (ANOVA) reported in Table 3, the specimen type was statistically significant whereas the vibration velocity was only slightly significant (significance between 5% and 10%). Hence, damping is possibly slightly higher at higher vibration velocities, as shown by the boxplots of Fig. 9. However, this should be further assessed by testing higher vibration velocities, that could not

be reached with the current setup. Despite the possible weak correlation between damping and vibration velocity, it can be concluded that the viscous damping model is adequate to describe lattice behaviour with good approximation.

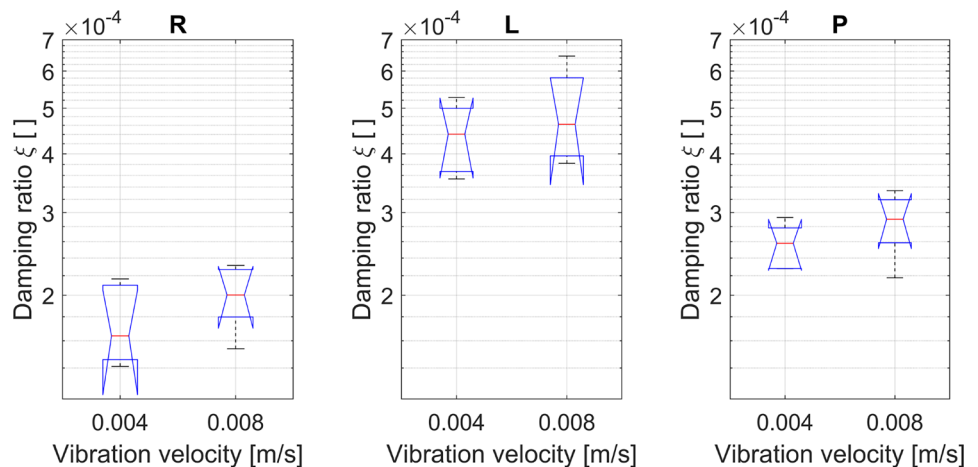
The inner damping capacity of a material is due to different damping mechanisms, which may depend on the reached strain amplitude [28]. For low strain amplitudes the amplitude independent internal friction is the main damping mechanism and energy is dissipated due to thermo-elastic currents and defects such as cracks, partially molten particles and spatters. Beyond a certain strain amplitude threshold, the amplitude dependent internal friction mechanisms (ADIF) become dominant. They become more effective with respect to amplitude independent mechanisms since energy dissipation is due to motion of dislocations and micro-plastic deformations.

When chirp pulsation is set to ω , the strain amplitude ϵ is implicitly given by:

$$\epsilon = \frac{\dot{\epsilon}}{\omega} \propto \frac{v_{rel}}{\omega} \cong \frac{const.}{\omega} \tag{2}$$

where v_{rel} is the relative vibration velocity between the specimen tip and the central clamping device, which is assumed constant during a single chirp test. Thus, the variation of vibration velocity amplitude v_{rel} allows to test different levels of strain amplitude ϵ , for a fixed pulsation ω . Since the correlation between vibration velocity and damping was weak, it is reasonable to assume that the critical strain amplitude

Fig. 9 Effect of vibration velocity variation on damping losses



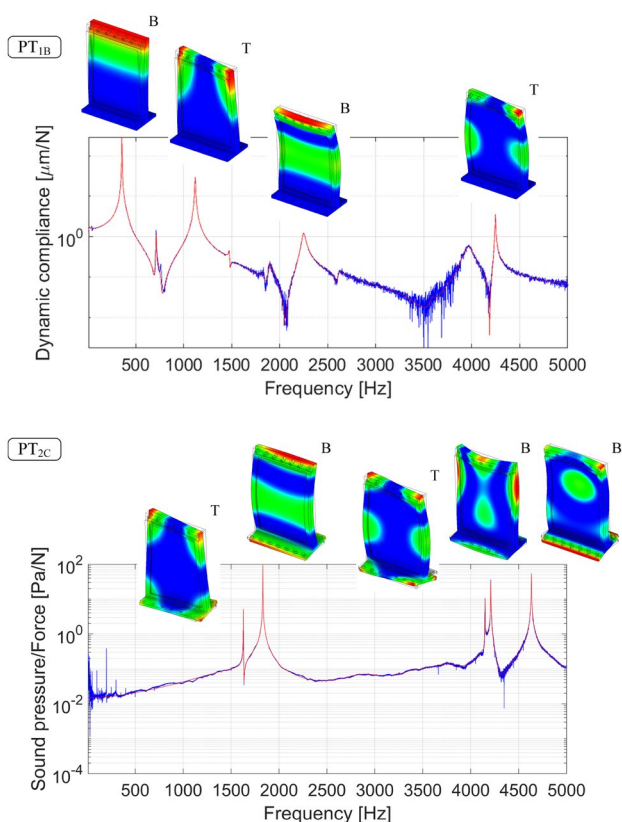


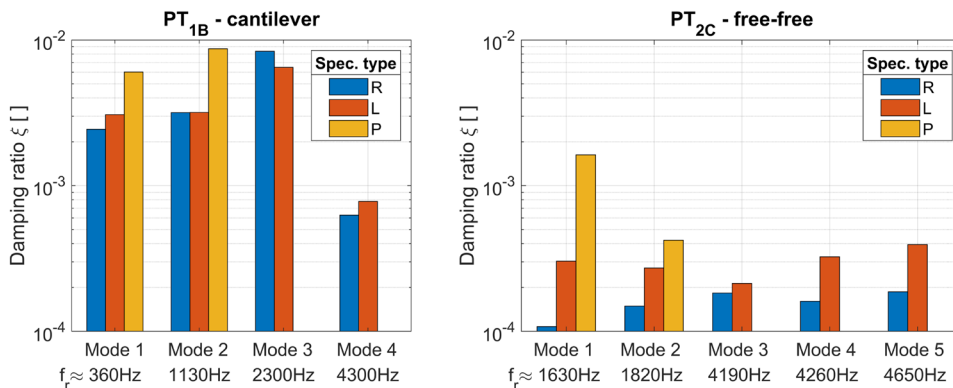
Fig. 10 Reference blade-like specimen (R) dynamic compliance

threshold ϵ_{cr} was not exceeded and the damping mechanisms were mostly amplitude independent. It is also reasonable to expect that under more severe operative conditions where $\epsilon > \epsilon_{cr}$, lattice structures could exhibit even better damping properties than those measured for small strain amplitudes.

Results Obtained from Blade-like Specimens

In the case of beam-like specimens, only the first dominant bending mode could be observed under the considered experimental conditions.

Fig. 11 Damping ratios of PT_{1B} and PT_{2C} configurations belonging to the vibration modes up to 5 kHz



On the contrary, blade-like specimens exhibited a richer dynamic behaviour characterized by many weakly damped bending and torsional modes in the range 100-5000 Hz. Thus, a thorough investigation of the associated damping ratios was carried out, in order to further explore the influence of lattice structures on thin-walled components. For this purpose, impulsive forces were applied both to the blade upper edge centre and corner, thus allowing an appropriate excitation of both bending and torsional modes.

The dynamic compliances of the reference blade-like specimen (R) measured in PT_{1B} and PT_{2C} configurations are shown in Fig. 10.

A parametric model interpolating the observed dynamic compliances was successfully identified through the IDS algorithm [38]. Finite Element Analysis allowed to recognize out-of-plane bending (B) and torsional (T) modes.

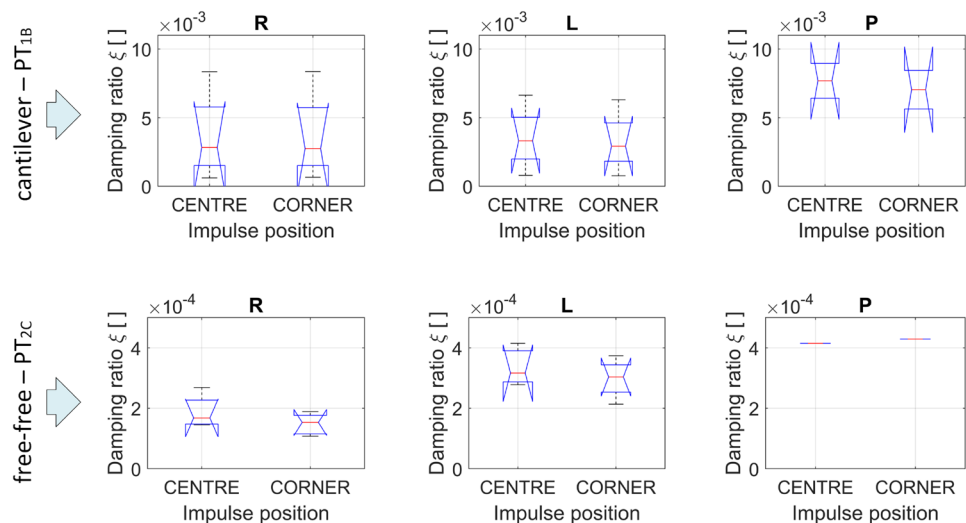
Figure 11 shows the damping ratios of the most important vibration modes. Some results regarding type P specimen are missing because they could not be detected due to a poor signal to noise ratio in the high-frequency range. Evaluating the experimental setup influence on lattice damping behaviour, considerations similar to those made for the beam-like specimens may also apply to the blade-like ones.

In PT_{1B} damping ratios were one order of magnitude higher because of the specimen-vice dynamic coupling. In such conditions type P was clearly superior than type R when considering the first bending and the first torsional vibration modes. Nevertheless, type L was not clearly better than R under such clamping conditions, as already noticed in [32].

The superior damping performance of P over L and of L over R was only revealed in the last PT_{2C} setup, where free-free boundary conditions are applied.

Damping ratio variance was greater when considering the results obtained from the cantilever configuration, because of the specimen-vice interactions, responsible for random and systematic damping losses due to contact phenomena. On the other side, the free-free conditions minimized the influence of external damping sources, thus enhancing repeatability.

Fig. 12 Influence of impulse position on damping ratio



Measurements repeatability was good since no appreciable effect on the specimens dynamic behaviour was detected when impulsive force application point was shifted between centre and corner. The boxplot of Fig. 12 as well as ANOVA on damping ratio with impulse position as factor confirm this outcome.

In short, the lattice metamaterial is characterized by higher internal damping. Moreover, internal damping losses are significantly higher when metal powder filler is present.

Conclusions

In this work, the dynamic behaviour of a given AISI 316L SLM lattice structure was experimentally investigated, by also focusing on a critical evaluation of the influence of external damping sources on the modal analysis outcomes.

The dynamic compliances of beam-like and blade-like specimens embedding a specific lattice structure with and without metal powder filler were measured under different clamping conditions and with several experimental setups.

Measurements confirmed the superior damping properties of lattice structures with respect to the full density reference material. Moreover, when the lattice structure was filled with unmelted metal powder, damping was further considerably enhanced.

The classical viscous damping model was confirmed to be valid with good approximation, although a weak dependence on vibration velocity was detected. However, amplitude independent internal friction mechanisms were dominant under the considered conditions.

Modal analysis performed in the anechoic chamber by suspending the specimens in free-free boundary conditions and by inspecting them through a microphone is

the most recommended configuration for a correct and accurate estimation of lattice internal damping.

On the contrary, the other setups for modal analysis were strongly affected by contact sensors (if any) and by the energy dissipation at the contact interfaces with the clamping devices.

In short, lattice structures may provide a superior damping performance and the metal powder filler can act as an effective damping booster. However, the contribution of the lattice structure to global damping strongly depends on the effective clamping conditions. Therefore it is highly recommended to experimentally assess the real advantage of embedding lattice structures into the mechanical system of interest, thoroughly evaluating the effect of unwanted external damping sources.

In the future it would be of further interest to explore some novel advanced applications of SLM lattice metamaterials where the observed properties may provide an effective advantage.

Acknowledgements The Laboratory for Advanced Mechatronics - LAMA FVG - of the University of Udine is gratefully acknowledged for technical support. LAMA FVG is an international research center for product and process innovation where the three universities of Friuli Venezia Giulia (Italy) cooperate for promoting R & D activities at academic and industrial level.

Funding Open access funding provided by Università degli Studi di Trieste within the CRUI-CARE Agreement.

Declarations

Conflicts of Interest The authors declare no conflict of interest.

Open Access This article is licensed under a Creative Commons Attribution 4.0 International License, which permits use, sharing, adaptation, distribution and reproduction in any medium or format, as long

as you give appropriate credit to the original author(s) and the source, provide a link to the Creative Commons licence, and indicate if changes were made. The images or other third party material in this article are included in the article's Creative Commons licence, unless indicated otherwise in a credit line to the material. If material is not included in the article's Creative Commons licence and your intended use is not permitted by statutory regulation or exceeds the permitted use, you will need to obtain permission directly from the copyright holder. To view a copy of this licence, visit <http://creativecommons.org/licenses/by/4.0/>.

References

- Tofail SA et al (2018) Additive manufacturing: scientific and technological challenges, market uptake and opportunities. *Mater Today* 21(1):22–37. <https://doi.org/10.1016/j.mattod.2017.07.001>
- Junk S, Klerch B, Hochberg U (2019) Structural Optimization in Lightweight Design for Additive Manufacturing. *Procedia CIRP* 84:277–282. <https://doi.org/10.1016/j.procir.2019.04.277>
- Rankouhi B et al (2020) Experimental validation and microstructure characterization of topology optimized, additively manufactured SS316L components. *Mater Sci Eng A* 776:139050. <https://doi.org/10.1016/j.msea.2020.139050>
- Pan C, Han Y, Lu J (2020) Design and optimization of lattice structures: a review. *Appl Sci* 10(18):6374. <https://doi.org/10.3390/app10186374>
- Li Z-H et al (2020) Mechanical properties of AlSi10Mg lattice structures fabricated by selective laser melting. *Mater Des* 192:108709. <https://doi.org/10.1016/j.matdes.2020.108709>
- Liu Y et al (2020) Enhanced fatigue characteristics of a topology-optimized porous titanium structure produced by selective laser melting. *Addit Manuf* 32:101060. <https://doi.org/10.1016/j.addma.2020.101060>
- Xu Y et al (2019) Mechanical properties tailoring of topology optimized and selective laser melting fabricated Ti6Al4V lattice structure. *J Mech Behav Biomed Mater* 99:225–239. <https://doi.org/10.1016/j.jmbbm.2019.06.021>
- Kang D et al (2019) Multi-lattice inner structures for high-strength and light-weight in metal selective laser melting process. *Mater Des* 175:107786. <https://doi.org/10.1016/j.matdes.2019.107786>
- Dong G, Tang Y, Li D, Zhao YF (2020) Design and optimization of solid lattice hybrid structures fabricated by additive manufacturing. *Addit Manuf* 33:101116. <https://doi.org/10.1016/j.addma.2020.101116>
- Zhao M et al (2020) Mechanical and energy absorption characteristics of additively manufactured functionally graded sheet lattice structures with minimal surfaces. *Int J Mech Sci* 167:105262. <https://doi.org/10.1016/j.ijmecsci.2019.105262>
- Du Y et al (2020) Laser additive manufacturing of bio-inspired lattice structure: forming quality, microstructure and energy absorption behavior. *Mater Sci Eng A* 773:138857. <https://doi.org/10.1016/j.msea.2019.138857>
- Ho J, Leong K, Wong T (2020) Additively-manufactured metallic porous lattice heat exchangers for air-side heat transfer enhancement. *Int J Heat Mass Transf* 150:119262. <https://doi.org/10.1016/j.ijheatmasstransfer.2019.119262>
- Takezawa A, Zhang X, Kato M, Kitamura M (2019) Method to optimize an additively-manufactured functionally-graded lattice structure for effective liquid cooling. *Addit Manuf* 28:285–298. <https://doi.org/10.1016/j.addma.2019.04.004>
- Ramadani R, Kegl M, Predan J, Belšak A, Pehan S (2018) Influence of Cellular Lattice Body Structure on Gear Vibration Induced by Meshing. *Strojniški vestnik - Journal of Mechanical Engineering* 64(10):611–620. <https://doi.org/10.5545/sv-jme.2018.5349>
- Syam WP et al (2018) Design and analysis of strut-based lattice structures for vibration isolation. *Precis Eng* 52:494–506. <https://doi.org/10.1016/j.precisioneng.2017.09.010>
- Sun X et al (2022) High damping capacity of alsi10mg-niti lattice structure interpenetrating phase composites prepared by additive manufacturing and pressureless infiltration. *J Alloys Compd* 905:164075. <https://doi.org/10.1016/J.JALLCOM.2022.164075>
- Maconachie T et al (2019) SLM lattice structures: properties, performance, applications and challenges. *Mater Des* 183:108137. <https://doi.org/10.1016/j.matdes.2019.108137>
- Zadpoor AA (2019) Mechanical performance of additively manufactured meta-biomaterials. *Acta Biomater* 85:41–59. <https://doi.org/10.1016/j.actbio.2018.12.038>
- Lei H et al (2019) Evaluation of compressive properties of SLM-fabricated multi-layer lattice structures by experimental test and μ -CT-based finite element analysis. *Mater Des* 169:107685. <https://doi.org/10.1016/j.matdes.2019.107685>
- Zhong T, He K, Li H, Yang L (2019) Mechanical properties of lightweight 316L stainless steel lattice structures fabricated by selective laser melting. *Mater Des* 181:108076. <https://doi.org/10.1016/j.matdes.2019.108076>
- Jin N et al (2019) Failure and energy absorption characteristics of four lattice structures under dynamic loading. *Mater Des* 169:107655. <https://doi.org/10.1016/j.matdes.2019.107655>
- Hazeli K, Babamiri BB, Indeck J, Minor A, Askari H (2019) Microstructure-topology relationship effects on the quasi-static and dynamic behavior of additively manufactured lattice structures. *Mater Des* 176:107826. <https://doi.org/10.1016/j.matdes.2019.107826>
- Köhnen P et al (2018) Mechanical properties and deformation behavior of additively manufactured lattice structures of stainless steel. *Mater Des* 145:205–217. <https://doi.org/10.1016/j.matdes.2018.02.062>
- Ma S et al (2019) Mechanical behaviours and mass transport properties of bone-mimicking scaffolds consisted of gyroid structures manufactured using selective laser melting. *J Mech Behav Biomed Mater* 93:158–169. <https://doi.org/10.1016/j.jmbbm.2019.01.023>
- Leary M et al (2018) Inconel 625 lattice structures manufactured by selective laser melting (SLM): Mechanical properties, deformation and failure modes. *Materials & Design* 157:179–199. <https://doi.org/10.1016/j.matdes.2018.06.010>
- Geng X, Lu Y, Liu C, Li W, Yue Z (2019) Fracture characteristic analysis of cellular lattice structures under tensile load. *Int J Solids Struct* 163:170–177. <https://doi.org/10.1016/j.ijsostr.2019.01.006>
- Andresen S, Bäger A, Hamm C (2020) Eigenfrequency maximisation by using irregular lattice structures. *J Sound Vib* 465:115027. <https://doi.org/10.1016/j.jsv.2019.115027>
- Rosa F, Manzoni S, Casati R (2018) Damping behavior of 316L lattice structures produced by Selective Laser Melting. *Materials & Design* 160:1010–1018. <https://doi.org/10.1016/j.matdes.2018.10.035>
- Haghshenas A, Khonsari M (2018) Evaluation of fatigue performance of additively manufactured SS316 via internal damping. *Manufacturing Letters* 18:12–15. <https://doi.org/10.1016/j.mfglet.2018.09.001>
- Sortino M, Totis G, Scalzo F, Vaglio E (2019) Preliminary Investigation of Static and Dynamic Properties of SLM Lattice Structures for Robotic Applications. In: Gasparetto A, Ceccarelli M (eds) *Mechanisms and Machine Science*, vol 66. Springer, Netherlands, pp 260–267
- Scalzo F, Totis G, Vaglio E, Sortino M (2021) Experimental study on the high-damping properties of metallic lattice structures obtained from SLM. *Precis Eng* 71:63–77. <https://doi.org/10.1016/j.precisioneng.2021.02.010>

32. Scalzo F, Totis G, Vaglio E, Sortino M (2020) Passive Chatter Suppression of Thin-Walled Parts by Means of High-Damping Lattice Structures Obtained from Selective Laser Melting. *Journal of Manufacturing and Materials Processing* 4(4):117. <https://doi.org/10.3390/jmmp4040117>
33. Hong Y, Guo K, Sun J, Yang B, Zhang C (2022) Investigation on vibration properties of 3D printed lattice structures filled with tin–bismuth alloy. *J Appl Phys* 131(6):065105. <https://doi.org/10.1063/5.0073251>
34. Li H et al (2021) Broadband low-frequency vibration attenuation in 3D printed composite meta-lattice sandwich structures. *Compos Part B Eng* 215:108772. <https://doi.org/10.1016/j.compositesb.2021.108772>
35. Liu J et al (2021) Compressive behavior and vibration-damping properties of porous Ti-6Al-4v alloy manufactured by laser powder bed fusion. *J Manuf Process* 66:1–10. <https://doi.org/10.1016/j.jmapro.2021.03.060>
36. Wang Q et al (2020) Effects of aging and thermal cycling on the microstructure and damping behaviors of a porous CuALMn shape memory alloy. *J Market Res* 9(4):7020–7026. <https://doi.org/10.1016/j.jmrt.2020.05.031>
37. Vanwalleghem J, De Baere I, Loccufer M, Van Paepegem W (2014) External damping losses in measuring the vibration damping properties in lightly damped specimens using transient time-domain methods. *J Sound Vib* 333(6):1596–1611. <https://doi.org/10.1016/j.jsv.2013.10.015>
38. Dombovari Z (2017) Dominant modal decomposition method. *J Sound Vib* 392:56–69. <https://doi.org/10.1016/j.jsv.2016.12.012>
39. Wojtowicki J-L, Jaouen L, Panneton R (2004) New approach for the measurement of damping properties of materials using the Oberst beam. *Rev Sci Instrum* 75(8):2569–2574. <https://doi.org/10.1063/1.1777382>
40. Duerinck T et al (2021) Experimental comparison of various excitation and acquisition techniques for modal analysis of violins. *Appl Acoust* 177:107942. <https://doi.org/10.1016/j.apacoust.2021.107942>

Publisher's Note Springer Nature remains neutral with regard to jurisdictional claims in published maps and institutional affiliations.